

Separated-beam nonphase-matched second-harmonic method of characterizing nonlinear optical crystals

Russell J. Gehr and A. V. Smith

Department 1128, Lasers, Optics, and Remote Sensing, Sandia National Laboratories, Albuquerque, New Mexico 87185-1423

Received January 28, 1998; revised manuscript received April 27, 1998

We demonstrate a variation of the wedge method of Maker-fringe measurement in which the fundamental beam diameter is large enough to contain several second-harmonic coherence fringes. In the far field the second harmonic forms spatially separated beams from which both Δk 's and d_{eff} 's can be deduced on a single laser pulse. Analysis is simple because no fringe analysis is required and because the method is immune to multiple surface reflections, birefringent walk-off, group-velocity walk-off, and surface effects such as longitudinal polarization. Example measurements on KDP and LiIO_3 are presented. © 1998 Optical Society of America [S0740-3224(98)00708-5]

OCIS codes: 160.4330, 190.4400, 190.2620.

1. INTRODUCTION

Among numerous methods of characterizing nonlinear optical crystals,¹ the Maker-fringe technique²⁻⁴ and its variations such as the translated-wedge method^{5,6} are the most commonly used. In the first demonstration, Maker *et al.*² measured second-harmonic strength while varying the incidence angle of the fundamental beam on a thin sample of uniform thickness. When a single nonlinear process is isolated by a proper choice of the fundamental and harmonic polarizations, this produces a pattern of harmonic fringes from which the coherence length and thus the phase-velocity mismatch, $\Delta k = k_{2\omega} - 2k_{\omega}$, can be deduced. By comparison of the strength of the fundamental and second-harmonic beams, the magnitude of the effective nonlinear coefficient, d_{eff} , can also be determined. Usually, however, only a relative value of d_{eff} is found by comparison to a reference crystal such as potassium dihydrogen phosphate (KDP).

The Maker-fringe method is complicated by etalon effects that are due to multiple reflections from the two parallel surfaces,^{4,7,8} and, for small beam diameters, by both birefringent walk-off and an angle-dependent walk-off that is proportional to the phase mismatch.³ Additionally, group-velocity walk-off is important for short pulses. The translated-wedge method^{5,6,8} overcomes some of these difficulties. The sample is wedged with an apex angle large enough to spoil the etalon for both the fundamental or harmonic waves, but small enough that the variation in sample thickness over the beam diameter is much less than a coherence length. Varying the sample thickness by translation rather than rotation eliminates the angular variation of d_{eff} as well as the angle-dependent walk-off. However, multiple reflections can still be a problem,^{7,8} as can birefringent and group-velocity walk-off.

In a variation of the wedge method, second-harmonic

microscopy of a wedged sample^{9,10} was used to characterize ferroelectric domains by use of a fundamental beam large enough to illuminate many coherence fringes. It is apparent that in this case the far-field harmonic light will form spatially separated beams, as was pointed out long ago by Bloembergen and Pershan.¹¹ That is the basis of the method we report here. The sample is cut as shown in Fig. 1 with the exit face sufficiently tilted that it cuts through several coherence lengths across the width of the fundamental beam. From the angles of the spatially separated far-field harmonic beams, a simple analysis yields refractive indexes, n_{ω} and $n_{2\omega}$, plus the phase-velocity mismatch, Δk . A measurement of the fundamental and harmonic irradiances, combined with the refractive indexes, yields d_{eff} . Further, different nonlinear processes associated with various combinations of fundamental and harmonic polarizations can sometimes create separate harmonic beams, permitting simultaneous characterization of multiple nonlinear processes, including relative signs of the associated nonlinear coefficients. We will show that because no fringe patterns are used, and because the boundary conditions on the optical fields are simple, accurate measurements can be accomplished quickly with minimal analysis. We will also show that this method is insensitive to birefringent and group-velocity walk-off.

2. THEORY FOR PLANE WAVES

We begin with a reminder that both the fundamental and harmonic waves have two orthogonal eigen polarizations in a crystal, with polarization directions determined by the crystal orientation. For any propagation direction there are six possible mixing processes, and thus six possible values of d_{eff} corresponding to eigen-polarization combinations $(1 \leftarrow 1, 1)$, $(1 \leftarrow 2, 1)$, $(1 \leftarrow 2, 2)$,

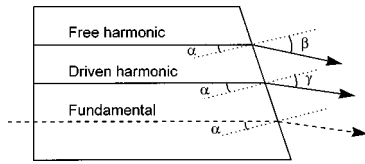


Fig. 1. Diagram of nonlinear crystal and the fundamental beam plus the free and driven harmonic beams.

$(2 \leftarrow 1, 1)$, $(2 \leftarrow 2, 1)$, and $(2 \leftarrow 2, 2)$. Here and throughout this paper the first number refers to the polarization of the second harmonic, while the second and third numbers represent polarizations of the fundamental waves. For uniaxial crystals, or for propagation in any principal plane of a biaxial crystal, the two eigen polarizations may be classified as ordinary, or o , and extraordinary, or e . It is usually possible to isolate individual mixing processes by proper choice of the fundamental and harmonic polarizations.

The generation of the second harmonic in a wedged sample is perhaps best described in terms of the driven and free second-harmonic plane waves that are often invoked in solving Maxwell's equations for plane-wave second-harmonic generation.^{3,5,11,12} The driven wave is the specific solution to the wave equation for second-harmonic generation in the limit of low conversion efficiency. It is tied in phase and amplitude to the harmonic polarization wave, giving it a propagation vector of $2\mathbf{k}_\omega$. The free wave is a general solution to the harmonic wave equation without the nonlinear source polarization, so it has the characteristics of a freely propagating second-harmonic wave with propagation vector $\mathbf{k}_{2\omega}$. In the absence of linear absorption, and in the plane-wave limit, the magnitudes of the two harmonic fields are constant over the length of the crystal and proportional to $d_{\text{eff}}E_\omega^2/\Delta k$, where E_ω is the fundamental field in the crystal. The phase and the amplitude of the free wave are adjusted so it very nearly cancels the driven wave at the input face of the crystal. Because the two waves propagate with different phase velocities, interference between them alternates between constructive and destructive through the length of the crystal. The nulls of the harmonic always parallel the crystal input face, spaced one coherence length apart, where the coherence length is defined by

$$L_c = 2\pi/\Delta k = 2\pi/|(\mathbf{k}_{2\omega} - 2\mathbf{k}_\omega)|. \quad (1)$$

In the customary Maker-fringe measurement, a parallel-sided crystal is rotated to change Δk , leading to oscillation of the output harmonic strength with crystal angle. If instead the output face of the crystal is tilted as in Fig. 1 so it cuts through several coherence lengths over the width of the beams, the Maker fringes will be washed out. However, the presence of several fringes of modulation over a beam diameter ensures that the harmonic wave is composed of two distinct angularly separated plane waves. This can be described more clearly by considering the driven and free waves separately. At the exit face the requirement that the component of the propagation vector parallel to the face be continuous across the crystal/air boundary (Snell's law) gives the exit

angles of the free and driven waves. The free wave has a propagation constant $2\omega n_{2\omega}/c$ so its exit angle, β , satisfies

$$\beta = \arcsin(n_{2\omega} \sin \alpha), \quad (2)$$

where α is the tilt of the exit face. The driven wave has propagation constant

$$2\bar{k}_\omega = (n_\omega + n'_\omega)\omega/c = 2\bar{n}_\omega\omega/c, \quad (3)$$

where n_ω and n'_ω are the refractive indexes for the two fundamental polarizations and \bar{n}_ω is their average value. The exit angle of the driven wave must satisfy

$$\gamma = \arcsin(\bar{n}_\omega \sin \alpha). \quad (4)$$

The angular separation of the two harmonic waves is

$$\delta = \beta - \gamma = \arcsin(n_{2\omega} \sin \alpha) - \arcsin(\bar{n}_\omega \sin \alpha). \quad (5)$$

Angle δ is usually small because the difference ($\bar{n}_\omega - n_{2\omega}$) is small, so it can be approximated by

$$\begin{aligned} \delta &= (n_{2\omega} - \bar{n}_\omega) \frac{\sin \alpha}{\sqrt{1 - \bar{n}_\omega^2 \sin^2 \alpha}} \\ &= \frac{\Delta k}{2k_0} \frac{\sin \alpha}{\sqrt{1 - \bar{n}_\omega^2 \sin^2 \alpha}}, \end{aligned} \quad (6)$$

where $k_0 = \omega/c$ and $\Delta k = k_{2\omega} - 2\bar{k}_\omega$. Thus the separation of the harmonic waves provides a measure of Δk assuming α and \bar{n}_ω are known.

According to Bloembergen and Pershan,¹¹ the amplitudes of the free and driven waves for normal incidence at the input face are

$$\begin{aligned} E_{\text{driven}} &= \frac{-P_{\text{par}}}{\epsilon_0(n_{2\omega}^2 - \bar{n}_\omega^2)}, \\ E_{\text{free}} &= \frac{P_{\text{par}}}{\epsilon_0(n_{2\omega}^2 - \bar{n}_\omega^2)} \left(\frac{\bar{n}_\omega + 1}{n_{2\omega} + 1} \right) \\ &= \frac{P_{\text{par}} 2k_0}{\epsilon_0(n_{2\omega} + \bar{n}_\omega)(\Delta k)} \left(\frac{\bar{n}_\omega + 1}{n_{2\omega} + 1} \right). \end{aligned} \quad (7)$$

The quantity P_{par} is the projection of the second-harmonic polarization along the direction of polarization of the harmonic wave,

$$P_{\text{par}} = \epsilon_0 d_{\text{eff}} E_\omega^2, \quad (9)$$

where d_{eff} is the effective nonlinear coefficient.¹ Examples of d_{eff} are listed in Tables 1–5. We assume in writing Eq. (8) that the fundamental light is linearly polarized at 45° relative to the eigen polarizations for a doubling process involving both e and o fundamental polarizations, or along an eigen polarization for a process involving one fundamental polarization. Note that the free-wave amplitude differs from the driven-wave amplitude by an amount equal to the reflected harmonic field.¹¹ Usually this difference is small. We neglect the influence of double refraction or birefringence, so the expression is exact only for mixing processes with no birefringent walk-

Table 1. $|d_{\text{eff}}|$ for Crystals Belonging to Symmetry Group 6 (LiIO₃) and Group 6mm (CdSe)^a

Polarizations	$ d_{\text{eff}} $ Group 6	$ d_{\text{eff}} $ Group 6mm
$o \leftarrow o, o$	0	0
$o \leftarrow o, e$	$d_{XXZ} S_\theta$	$d_{XXZ} S_\theta$
$o \leftarrow e, e$	$d_{XYZ} S_{2\theta}$	0
$e \leftarrow o, o$	$d_{ZXX} S_\theta$	$d_{ZXX} S_\theta$
$e \leftarrow o, e$	$\frac{1}{2} d_{XYZ} S_{2\theta}$	0
$e \leftarrow e, e$	$(2d_{XXZ} + d_{ZXX})C_\theta^2 S_\theta + d_{ZZZ} S_\theta^3$	$(2d_{XXZ} + d_{ZXX})C_\theta^2 S_\theta + d_{ZZZ} S_\theta^3$

^a S_θ is $\sin \theta$, and C_θ is $\cos \theta$.**Table 2.** $|d_{\text{eff}}|$ for Crystals Belonging to Symmetry Group $\bar{4}2m$ (KDP, AgGaS₂, AgGaSe₂, ZnGeP₂, CdGeAs₂) and Group 3m (β -BaB₂O₄, LiNbO₃)

Polarizations	$ d_{\text{eff}} $ Group $\bar{4}2m$	$ d_{\text{eff}} $ Group 3m
$o \leftarrow o, o$	0	$d_{YYY} C_{3\phi}$
$o \leftarrow o, e$	$d_{XYZ} S_\theta S_{2\phi}$	$d_{XXZ} S_\theta - d_{YYY} C_\theta S_{3\phi}$
$o \leftarrow e, e$	$d_{XYZ} S_{2\theta} C_{2\phi}$	$d_{YYY} C_\theta^2 C_{3\phi}$
$e \leftarrow o, o$	$d_{ZXY} S_\theta S_{2\phi}$	$d_{ZXX} S_\theta - d_{YYY} C_\theta S_{3\phi}$
$e \leftarrow o, e$	$\frac{1}{2} (d_{XYZ} + d_{ZXY}) S_{2\theta} C_{2\phi}$	$d_{YYY} C_\theta^2 C_{3\phi}$
$e \leftarrow e, e$	$(2d_{XYZ} + d_{ZXY}) C_\theta^2 S_\theta S_{2\phi}$	$d_{ZZZ} S_\theta^3 + (2d_{XXZ} + d_{ZXX}) C_\theta^2 S_\theta + d_{YYY} C_\theta^3 S_{3\phi}$

Table 3. $|d_{\text{eff}}|$ for KTP Family in the Optical Frame (x, y, z)

Polarizations	$ d_{\text{eff}} $ xz Plane	$ d_{\text{eff}} $ xy Plane	$ d_{\text{eff}} $ yz Plane
$o \leftarrow o, o$	0	d_{zzz}	0
$o \leftarrow o, e$	$d_{yyz} S_\theta$	0	$d_{xxz} S_\theta$
$o \leftarrow e, e$	0	$d_{zxx} S_\phi^2 + d_{zyy} C_\phi^2$	0
$e \leftarrow o, o$	$d_{zyy} S_\theta$	0	$d_{zxx} S_\theta$
$e \leftarrow o, e$	0	$d_{xxz} S_\phi^2 + d_{yyz} C_\phi^2$	0
$e \leftarrow e, e$	$d_{zzz} S_\theta^3 + (2d_{xxz} + d_{zxx}) C_\theta^2 S_\theta$	0	$d_{zzz} S_\theta^3 + (2d_{yyz} + d_{zyy}) C_\theta^2 S_\theta$

Table 4. $|d_{\text{eff}}|$ for KNbO₃ in the Optical Frame (x, y, z)

Polarizations	$ d_{\text{eff}} $ xz Plane	$ d_{\text{eff}} $ yz Plane	$ d_{\text{eff}} $ xy Plane
$o \leftarrow o, o$	0	d_{xxx}	0
$o \leftarrow o, e$	$d_{yyx} C_\theta$	0	$d_{zxx} S_\phi$
$o \leftarrow e, e$	0	$d_{xyy} C_\theta^2 + d_{xzz} S_\theta^2$	0
$e \leftarrow o, o$	$d_{xyy} C_\theta$	0	$d_{xzz} S_\phi$
$e \leftarrow o, e$	0	$d_{yyx} C_\theta^2 + d_{zxx} S_\theta^2$	0
$e \leftarrow e, e$	$d_{xxx} C_\theta^3 + (2d_{zxx} + d_{xzz}) S_\theta^2 C_\theta$	0	$d_{xxx} S_\phi^3 + (2d_{yyx} + d_{xyy}) C_\phi^2 S_\phi$

Table 5. $|d_{\text{eff}}|$ for LiB₃O₅ in the Optical Frame (x, y, z)

Polarizations	$ d_{\text{eff}} $ xy Plane	$ d_{\text{eff}} $ xz Plane	$ d_{\text{eff}} $ yz Plane
$o \leftarrow o, o$	0	d_{yyy}	0
$o \leftarrow o, e$	$d_{zzy} C_\phi$	0	$d_{xxy} C_\theta$
$o \leftarrow e, e$	0	$d_{yxx} C_\theta^2 + d_{yzz} S_\theta^2$	0
$e \leftarrow o, o$	$d_{yzz} C_\phi$	0	$d_{yxx} C_\theta$
$e \leftarrow o, e$	0	$d_{xxy} C_\theta^2 + d_{zzy} S_\theta^2$	0
$e \leftarrow e, e$	$d_{yyy} C_\phi^3 + (2d_{xxy} + d_{yxx}) S_\phi^2 C_\phi$	0	$d_{yyy} C_\theta^3 + (2d_{zzy} + d_{yzz}) S_\theta^2 C_\theta$

off, for example, an ($o \leftarrow o, o$) process, or any process if the crystal's optic axis is aligned parallel or perpendicular to the light propagation direction. In a later section we will present corrections that account for birefringent walk-off.

Equations (7) and (8) are valid in the presence of linear absorption if the n 's are replaced by $(n + i\kappa)$'s where the κ 's are linear extinction indexes. Equation (8) then gives the free field at the crystal input face, $E_{\text{free}}(0)$. The free wave decays according to

$$E_{\text{free}}(z) = E_{\text{free}}(0)\exp(-2k_0\kappa_{2\omega}z). \quad (10)$$

The driven wave, in contrast, is tied to the driving harmonic polarization and so decays according to

$$E_{\text{driven}}(z) = E_{\text{driven}}(0)\exp[-(\kappa_\omega + \kappa'_\omega)k_0z]. \quad (11)$$

3. THEORY FOR GAUSSIAN SPATIAL AND TEMPORAL PROFILES

Light beams that are limited in space and time can be decomposed into properly phased monochromatic plane waves of varying propagation direction and frequency. Each of the plane waves constituting the harmonic polarization beam will have associated with it the driven and free plane-wave pair that satisfy Eqs. (7) and (8). If the variation in Δk over the angular and frequency range of the polarization beam is much less than the carrier mismatch, Δk , the denominator of Eq. (8) is nearly constant for all the constituent free plane waves. In that case the composite free wave at the input face has the same amplitude and phase profile as the harmonic polarization at the input face, both spatially and temporally. The propagation of the free wave thereafter, being that of a freely propagating harmonic wave, is subject to the usual linear absorption, birefringent walk-off, and group-velocity effects. At the exit face it will have the same beam profile and irradiance as that expected for linear propagation of the free wave as it existed at the input face. Clearly the pulse energy of the free wave is unaffected by birefringent or group-velocity walk-off effects, and its strength can be easily related to the nonlinear coefficient, d_{eff} .

The requirement of small variation in Δk over the constituent waves can be related to known crystal parameters. For example, assuming an input beam with a Gaussian spatial profile of radius R , with a confocal parameter much larger than the crystal length, the restriction on angular range may be expressed as

$$\Delta k \gg \frac{\rho}{R}, \quad (12)$$

where ρ is the birefringent walk-off angle. Similarly, the requirement on the group-velocity walk-off is

$$\Delta k \gg \frac{\sigma}{\tau}, \quad (13)$$

where τ is the pulse duration and σ is the group-velocity walk-off expressed as a separation time per propagation length. In other words, both walk-off lengths must be many coherence lengths.

If these conditions are met, it is straightforward to show that for a pulsed, weakly focused beam described by

$$E_\omega(r, t) = E_0 \exp(-t^2/\tau^2)\exp(-r^2/R^2), \quad (14)$$

in the low conversion limit the pulse energy of the free wave outside the exit face of the crystal is

$$U_{\text{free}} = U_\omega^2 \frac{2d_{\text{eff}}^2}{\pi^{3/2}\tau R^2 \epsilon_0 c} \left| \frac{\bar{n}_\omega + 1}{n_{2\omega} + 1} \right|^2 \left| \frac{2k_0}{(n_{2\omega} + \bar{n}_\omega)(\Delta k)} \right|^2 |t_\omega|^2 |t'_\omega|^2 |t_{2\omega}|^2 \exp(-2\kappa_{2\omega}\omega L/c), \quad (15)$$

where U_ω is the fundamental pulse energy incident on the crystal, the n 's are in general of the form $n + i\kappa$, and L is the crystal length. The t_ω 's are transmission coefficients for the fundamental electric field at the crystal entrance face given by

$$t_\omega = \frac{2}{1 + n_\omega}, \quad (16)$$

$$t'_\omega = \frac{2}{1 + n'_\omega}, \quad (17)$$

while $t_{2\omega}$ is the transmission coefficient for the harmonic at the exit face given by

$$t_{2\omega} = \frac{2n_{2\omega} \cos \alpha}{n_{2\omega} \cos \alpha + \cos \beta} \quad (18)$$

for an s -polarized free wave, or

$$t_{2\omega} = \frac{2n_{2\omega} \cos \alpha}{n_{2\omega} \cos \beta + \cos \alpha} \quad (19)$$

for a p -polarized free wave. Using Eqs. (14)–(19), a measurement of the input fundamental energy and the output harmonic energy in the free wave gives the value of d_{eff} assuming the other crystal and beam parameters are known.

We could also derive exact expressions relating d_{eff} to the strength of the driven wave. However, this requires the application of more complex boundary conditions at the exit face. There will be reflected fundamental waves leading to associated driven and free waves, plus a reflected free wave from the incident driven wave, in addition to the incident and transmitted driven waves. Chemla and Kupecek⁵ have derived the driven-wave transmission coefficient where all the waves are s polarized. For p polarizations the situation is more complicated because the reflected waves can experience a change in refractive index in birefringent crystals and, if the harmonic is p polarized, the longitudinal component of the nonlinear polarization must also be considered. As Bloembergen and Pershan¹¹ pointed out, these are all essentially surface effects so only a fraction of a wavelength of the crystal contributes to them, in contrast to the main contribution from one coherence length of crystal. In most cases, the difference between the free and driven waves will be only a few percent, usually within the accu-

racy of the measurement, but by basing the measurement of d_{eff} on the free-wave energy alone, such effects are entirely eliminated.

Another advantage of using only the free wave is that its energy is independent of walk-off effects, whereas that of the driven wave is not. The free wave may be considered to arise at the input face, while the driven wave can be considered to arise at the exit face. In $(e \leftarrow o, o)$ or $(o \leftarrow e, e)$ doubling, the driven and free waves are spatially offset at the exit face; in the first case because the free wave generated at the entrance face experiences walk-off, while the driven wave generated at the exit face overlaps the fundamental wave that does not walk off; in the second case because the harmonic wave does not walk off while the fundamental does. In Maker-fringe measurements the overlap between the free and driven waves is reduced by spatial walk-off, affecting the degree of interference between them, complicating analysis. Our method eliminates this interference, making it insensitive to walk-off. If the fundamental beams separate, as they can in $(e \leftarrow o, e)$ or $(o \leftarrow o, e)$ doubling, the polarization wave and thus the driven wave will be reduced or even eliminated at the exit face, in which case only the free wave emerges. This discussion of spatial walk-off applies in an obvious way to temporal walk-off with spatial separation replaced by temporal separation. For example, if the fundamental beams are of the same polarization and so have identical group velocities, while the harmonic has a different group velocity, the free and driven pulses will emerge separated in time. If the separation is large compared with the pulse duration, they cannot interfere, making Maker-fringe measurements impossible. Typical temporal walk-off is hundreds of femtoseconds per millimeter, so this is an issue for picosecond and shorter pulses. Using our method, a complete measurement is unhampered. In a later section we present a laboratory measurement demonstrating birefringent walk-off effects.

Finally, we note that associated with the combination of spatial (temporal) walk-off and nonzero Δk there is a tilt (frequency shift) of order $\rho/k\Delta kR^2$ ($\sigma/\Delta k\tau^2$). If the conditions specified in Eqs. (12) and (13) are met, these tilts and shifts will be much smaller than the angular (frequency) spread of the beam (pulse) and can be ignored. We have verified all described walk-off effects using a numerical model¹³ of frequency doubling.

4. BIREFRINGENT CORRECTIONS

If an e wave propagates at an angle to the optic axis, it experiences birefringent walk-off in which the Poynting vector, \mathbf{S} , is tilted by the walk-off angle, ρ , away from the propagation vector, \mathbf{k} . The electric field of the wave is perpendicular to \mathbf{S} rather than to \mathbf{k} , as was assumed in the derivations above. This difference requires slight corrections to the transmission coefficients, the free-wave amplitude, and the interpretation of d_{eff} . It is straightforward to apply the usual boundary conditions to derive the modified entrance-face transmission coefficient for an e -polarized fundamental wave as

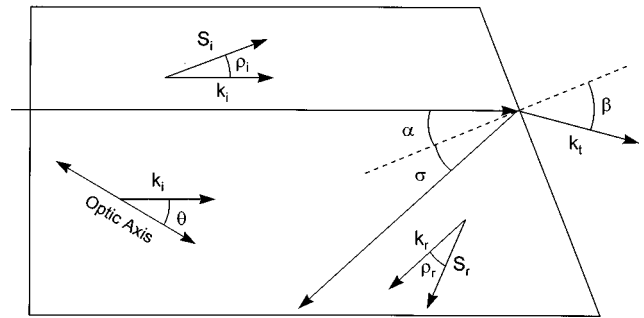


Fig. 2. Diagram of propagation in a birefringent crystal with its optic axis tilted in the same plane as the exit face. Poynting vectors of the incident and reflected waves are labeled S_i and S_r , respectively. The ρ 's are walk-off angles.

$$t_{\omega} = \frac{2}{\cos \rho + n_{\omega} \cos \rho}. \quad (20)$$

The o -wave coefficient is unmodified. A similar exercise yields the modified exit coefficient. If the optic axis and the tilt of the exit face lie in the same plane, as diagrammed in Fig. 2, an e wave is also a p wave, and the exit transmission coefficient for the harmonic wave becomes

$$t_{2\omega} = \frac{n_r \cos(\alpha + \rho_i) \cos \rho_r + n_i \cos(\sigma + \rho_r) \cos \rho_i}{n_r \cos \beta \cos \rho_r + \cos(\sigma + \rho_r)}, \quad (21)$$

where i and r refer to the incident and reflected fields at the exit face, and σ is the reflection angle. If birefringence decreases the tilt of the optical electric field relative to the exit face, as it does for the incident wave in Fig. 2, the sign of ρ is negative; otherwise, it is positive, as shown for the reflected wave. Note that for the reflected wave, the refractive index, reflection angle, and walk-off angle are different from those of the incident wave because the angle between the propagation direction and the optic axis changes. Both the reflection angle, σ , and refractive index, n_r , must be determined graphically or numerically by iteration. If the optic axis lies out of the plane of the exit-face tilt, the transmission coefficient is more complex, and we have not derived the relevant expressions. However, we will show in examples in the next two sections of this paper that the change in transmission coefficient owing to birefringence is usually negligible.

We account for the effect of birefringent-field tilts in relating d_{eff} to the d_{ijk} 's ($d_{ijk} = \chi_{ijk}/2$) by interpreting the angle θ in Tables 1 and 2 as the tilt of the Poynting vector rather than the tilt of the propagation vector. For negative uniaxial crystals the Poynting vector tilts away from the optic axis relative to the propagation vector, so θ is replaced by $(\theta + \rho)$. For positive uniaxial crystals, $\theta \rightarrow (\theta - \rho)$. The ϕ 's are unchanged. For biaxial crystals, $\theta \rightarrow (\theta - \rho)$ and $\phi \rightarrow (\phi + \rho)$ in Tables 3–5.

Finally, the driven-wave solution⁴ to the second-harmonic Maxwell equation is modified by birefringence. The solution to the wave equation

$$\nabla \times \nabla \times \mathbf{E}_{2\omega} - 4k_0^2 \bar{\epsilon} \cdot \mathbf{E}_{2\omega} = 4 \frac{k_0^2}{\epsilon_0} \mathbf{P}_{NL} \exp(i2\mathbf{k}_{\omega} \cdot \mathbf{r}) \quad (22)$$

is

$$\mathbf{E}_{\text{driven}} = \frac{-n_{2\omega}^2}{\epsilon_0(n_{2\omega}^2 - \bar{n}_\omega^2)} \left[\tilde{\epsilon}^{-1} \cdot \mathbf{P}_{NL} - \frac{\bar{\mathbf{k}}_\omega(\bar{\mathbf{k}}_\omega \cdot \mathbf{P}_{NL})}{(k_o n_o n_e)^2} \right], \quad (23)$$

where $\tilde{\epsilon}$ is the dielectric tensor, and n_o and n_e are the ordinary and extraordinary refractive indexes at the harmonic frequency. The free wave has the form

$$\mathbf{E}_{\text{free}} = A \tilde{\epsilon}^{-1} \cdot \hat{t}, \quad (24)$$

where \hat{t} is a unit vector parallel to the crystal input face. Applying the boundary conditions on the free, driven, and reflected harmonic waves at the input face¹¹ gives

$$\mathbf{E}_{\text{free}} = \frac{P_{\text{par}}}{\epsilon_0(n_{2\omega}^2 - \bar{n}_\omega^2)} \left(\frac{\bar{n}_\omega + 1}{n_{2\omega} + 1} \right) \times \left[n_{2\omega}^4 \left(\frac{\cos^2 \theta}{n_o^4} + \frac{\sin^2 \theta}{n_e^4} \right) \right], \quad (25)$$

where P_{par} is the projection of the nonlinear polarization along the electric field of the free wave, given by

$$P_{\text{par}} = \epsilon_0 d_{\text{eff}} E_\omega^2, \quad (26)$$

with the interpretation of d_{eff} just described. The birefringent correction is contained in the square brackets. Note that if the free wave is o polarized, the earlier expression for \mathbf{E}_{free} holds, but with the present interpretation of d_{eff} . In the next two sections we present examples comparing analysis with and without the birefringent corrections.

5. CHARACTERIZATION OF KDP

Because KDP is the standard against which nonlinear crystals are usually measured, it makes sense to demonstrate our method with an absolute measurement of d_{xyz} for KDP. We used an uncoated KDP sample cut for propagation along ($\theta = 75^\circ$, $\phi = 45^\circ$). As shown in Table 2, this cut permits three mixing processes: ($o \leftarrow o, e$), ($e \leftarrow o, o$), and ($e \leftarrow e, e$). We measured d_{eff} for the latter two and from them deduced d_{xyz} .

First we measured the exit-face tilt to be $\alpha = 14.3^\circ$ by aligning the crystal to retroreflect a helium–neon laser beam off the input face, rotating it 180° , and measuring the deflection of the beam reflected from the tilted face. The crystal was then placed in the beam of a pulsed Nd:YAG laser and adjusted so the untilted input face retroreflected the 1064-nm beam. The Nd:YAG laser was injection seeded for single-longitudinal-mode operation, and its beam was spatially filtered by focusing through a

diamond pinhole to produce a beam that was nearly Gaussian both spatially and temporally. The spatial profile was monitored by use of a video-camera-based beam profiler; the time profile was monitored by use of a photo-detector and oscilloscope with combined 1-GHz bandwidth. A half-wave retarder before the pinhole controlled the polarization in conjunction with a cleanup polarizer just before the crystal. Typical operating conditions were 11-ns pulse duration (FWHM), 0–10-mJ pulse energy, and 0.5-mm diameter. We did not measure the refractive indices directly in this case but rather used reliable Sellmeier values.¹⁴ We did measure Δk directly, however. With the input light polarized so both e and o fundamental waves were present, five second-harmonic beams were generated, corresponding to three driven waves with effective refractive indices n_ω^o , $n_\omega^e(\theta = 75^\circ)$, and $0.5[n_\omega^o + n_\omega^e(\theta = 75^\circ)]$, and two free waves with refractive indices of $n_{2\omega}^o$ and $n_{2\omega}^e(\theta = 75^\circ)$. The tilt angles of these beams were measured by placing a one-meter focal-length lens at the crystal exit face and measuring the separation of the beams one meter from the lens. This gives the relevant δ 's, from which the Δk 's can be derived according to Eq. (6). Our measured Δk 's agree with those calculated from the Sellmeier equations within 2%, as shown in Table 6.

For the measurement of d_{eff} , we polarized the input either e or o and measured the pulse energy in the free wave of interest using a photomultiplier. An aperture in front of the phototube selected the free wave of interest. Based on measured input and output pulse energies, plus measured input-beam diameter and pulse duration, along with the measured values of Δk , we derived the d_{eff} 's listed in Table 6 using Eq. (15). Both the 532-nm and 1064-nm pulse energies were referenced to a thermopile detector and to a pyroelectric detector, both calibrated within 5%. We note that the birefringent corrections to d_{eff} are negligible in this case, being much less than 1%. However, in converting from d_{eff} to d_{xyz} , birefringent corrections are a few percent owing to the walk-off angles of 0.65° for the fundamental and 0.78° for the harmonic. We used the average of these to adjust θ from 75° to 75.72° in the conversion. We find $d_{xyz} = 0.396 \pm 0.03$ pm/V from the ($e \leftarrow e, e$) measurement and $d_{xyz} = 0.387 \pm 0.03$ pm/V from the ($e \leftarrow o, o$) measurement, which together give a best value of 0.39 ± 0.03 pm/V, in agreement with the established value⁸ of 0.39 pm/V. Estimated error sources are refractive indices (1%), Δk (2%), spatial and temporal beam profile (2%), and energy calibrations (5%). Our best estimate of the overall accuracy is $\pm 7\%$.

Table 6. Comparison of Measured and Calculated Δk 's and d_{eff} 's for $\theta = 75^\circ$ KDP

Polarizations	Δk_{meas} (μm^{-1})	Δk_{calc} (μm^{-1}) ^a	$d_{\text{eff}}^{\text{meas}}$ (pm/V)	$d_{\text{eff}}^{\text{calc}}$ (pm/V) ^b
$e \leftarrow e, e$	$0.134 \pm 2\%$	0.131	0.073 ± 0.007	0.070
$e \leftarrow o, o$	$-0.244 \pm 2\%$	-0.245	0.375 ± 0.04	0.378

^aFrom Sellmeier equations of Ref. 14.

^bUsing $d_{xyz} = 0.39$ pm/V.

6. CHARACTERIZATION OF A $\theta = 23^\circ$ CUT LiIO₃ CRYSTAL

We used an identical method to measure d_{eff} 's for LiIO₃ cut for $\theta = 23^\circ$ propagation, except in this case we added a measurement of the refractive indices based on beam deflections. We measured an exit-face tilt of $\alpha = 12.50 \pm 0.05^\circ$ with the face normal lying in the extraordinary plane, as shown in Fig. 2 with $\theta = 23^\circ$. The exit angles of the transmitted fundamental beams and the crystal-

Table 7. Comparison of Measured and Calculated n 's and Δk 's for $\theta = 23^\circ$ LiIO₃

Polarizations	n_{meas}^{532}	n_{calc}^{532}	$\bar{n}_{\text{meas}}^{1064}$	$\bar{n}_{\text{calc}}^{1064}$	$\Delta k_{\text{meas}}(\mu\text{m}^{-1})$	$\Delta k_{\text{calc}}(\mu\text{m}^{-1})^a$
$e \leftarrow e, e$	$1.868 \pm 1\%$	1.87255	$1.832 \pm 1\%$	1.83317	$0.468 \pm 2\%$	0.4651
$e \leftarrow o, o$	$1.868 \pm 1\%$	1.87255	$1.854 \pm 1\%$	1.85686	$0.186 \pm 2\%$	0.1853
$o \leftarrow e, o$	$1.899 \pm 1\%$	1.89799	$1.843 \pm 1\%$	1.84502	$0.628 \pm 2\%$	0.6258

^aAll calculated values in this table are based on the Sellmeier equation of Ref. 15.

Table 8. Comparison of Measured d 's for LiIO₃

d_{ijk}	Value (pm/V)	Authors and Method
d_{xyz}	0.19 ± 0.06	This work
	0.2	Okada and Ieiri ^a : phase-matched second-harmonic generation (SHG), 1064 nm; relative to d_{zxx} of LiIO ₃
d_{zxx}	4.2 ± 0.3	This work: absolute measurement of ($e \leftarrow o, o$)
	4.3 ± 0.3	This work: ($e \leftarrow e, e$) relative to ($e \leftarrow o, o$) of LiIO ₃
	4.6 ± 0.2	This work: ($e \leftarrow o, o$) relative to ($e \leftarrow o, o$) of KDP
	4.1 ± 0.2	Eckardt <i>et al.</i> ^b : phase-matched SHG, 1064 nm; absolute and relative to KDP
	7.33	Choy and Byer ^c : parametric fluorescence, 514-nm pump; absolute
	4.4	Choy and Byer ^d : wedge method, nonphase-matched SHG, 1318 nm; relative to KDP
	4.65	Jerphagnon ^e : Maker-fringe, nonphase-matched SHG, 1064 nm; relative to quartz
d_{zzz}	12.1	Nath and Haussühl ^f : phase-matched SHG, 1064 nm; relative to KDP
	7.5	Campillo and Tang ^g : parametric fluorescence, 514-nm pump; absolute
	4.4	Choy and Byer ^h : wedge method, nonphase-matched SHG, 1318 nm; relative to KDP
	4.8	Jerphagnon ⁱ : Maker-fringe, nonphase-matched SHG, 1064 nm; relative to quartz

^a Ref. 16.

^b Ref. 19.

^c Ref. 6.

^d Ref. 6.

^e Ref. 17.

^f Ref. 20.

^g Ref. 21.

^h Ref. 6.

ⁱ Ref. 17.

generated second-harmonic beams yielded the refractive indices and Δk 's listed in Table 7. For comparison we list values calculated from the Sellmeier equations of Kato¹⁵ as well. The agreement between measured and calculated values is considerably better than the estimated error limits of the measurements, with differences generally less than 0.5%. We will use only our measured values in the analysis.

LiIO₃ belongs to symmetry group 6 for which the nonlinear tensor has the form¹

$$d = \begin{bmatrix} 0 & 0 & 0 & d_{xyz} & d_{xxz} & 0 \\ 0 & 0 & 0 & d_{xxz} & -d_{xyz} & 0 \\ d_{zxx} & d_{zxx} & d_{zzz} & 0 & 0 & 0 \end{bmatrix}. \quad (27)$$

The nonlinearity for this crystal class is independent of ϕ , so directions x and y are interchangeable. We do not know the ϕ cut of our crystal so, to simplify the discussion, we assume propagation is in the x - z plane. If Kleinman symmetry held, d_{xyz} would be zero and d_{zxx} would equal d_{xxz} . In fact, Okada and Ieiri¹⁶ measured $|d_{xyz}/d_{zxx}| = 0.05$ for doubling 1064-nm light so Kleinman symmetry is apparently not exact in LiIO₃ at our wavelengths, prompting us to maintain the distinction between d_{zxx} and d_{xxz} in our analysis. As Table 1 shows, there are five second-harmonic processes, but only the ($e \leftarrow e, e$), ($e \leftarrow o, o$), and ($o \leftarrow e, o$) processes are directly measurable because of the weakness of the two that

rely on d_{xyz} . We made an absolute measurement of the ($e \leftarrow o, o$) process and find $d_{\text{eff}} = 1.87$ pm/V, which translates to $d_{zxx} = 4.2 \pm 0.3$ pm/V. We also made the following relative measurements: ($e \leftarrow o, o$) in LiIO₃ relative to ($e \leftarrow o, o$) in KDP; ($e \leftarrow e, e$) in LiIO₃ relative to ($e \leftarrow o, o$) in LiIO₃; and ($o \leftarrow o, e$) in LiIO₃ relative to ($e \leftarrow o, o$) in LiIO₃.

The free wave of the ($o \leftarrow o, e$) process can interfere with that of the weak ($o \leftarrow e, e$) process, which is dependent on d_{xyz} . To test for this we compared harmonic signals with the fundamental polarized at 45° and at -45° relative to the o direction. The relative signs of the ($o \leftarrow e, e$) and ($o \leftarrow o, e$) free waves reverse with this angle change so comparison of the harmonic signals reveals their relative contributions. We find there is a significant contribution from the weak ($o \leftarrow e, e$) process and deduce a ratio $d_{xyz}/d_{zxx} = 0.043 \pm 0.015$, in good agreement with that reported by Okada and Ieiri.¹⁶ Removing the contribution of d_{xyz} , we find $d_{\text{eff}}(o \leftarrow o, e)/d_{\text{eff}}(e \leftarrow o, o) = 0.98$, indicating that $d_{xxz} = d_{zxx}$ within our measurement accuracy. We also found $d_{\text{eff}}(e \leftarrow e, e)/d_{\text{eff}}(e \leftarrow o, o) = 2.69$.

The walk-off angles according to Kato's Sellmeier equations¹⁵ are 3.42° at 1064 nm and 3.59° at 532 nm, so we used $\rho = 3.50^\circ$ in making the following birefringent corrections: the entrance transmission coefficient for e -polarized light increases by 1.002, the exit-face transmission coefficient increases by 1.007, and the correction fac-

tor in square brackets in Eq. (25) is 1.004. The net effect of these three corrections is to lower d_{eff} as deduced by use of Eqs. (15)–(19) by 1.5%, 1.1%, and 0.2%, respectively, for $(e \leftarrow e, e)$, $(e \leftarrow o, o)$, and $(o \leftarrow e, o)$. These birefringent corrections are included in deriving the ratios above.

Our results translate to the following values for d 's: $d_{zxx} = 4.2 \pm 0.3$ pm/V from the absolute measurement of $(e \leftarrow o, o)$, or $d_{zxx} = 4.6 \pm 0.2$ pm/V from the measurement relative to KDP; $d_{zxx} = 4.3 \pm 0.3$ from $(e \leftarrow e, e)$

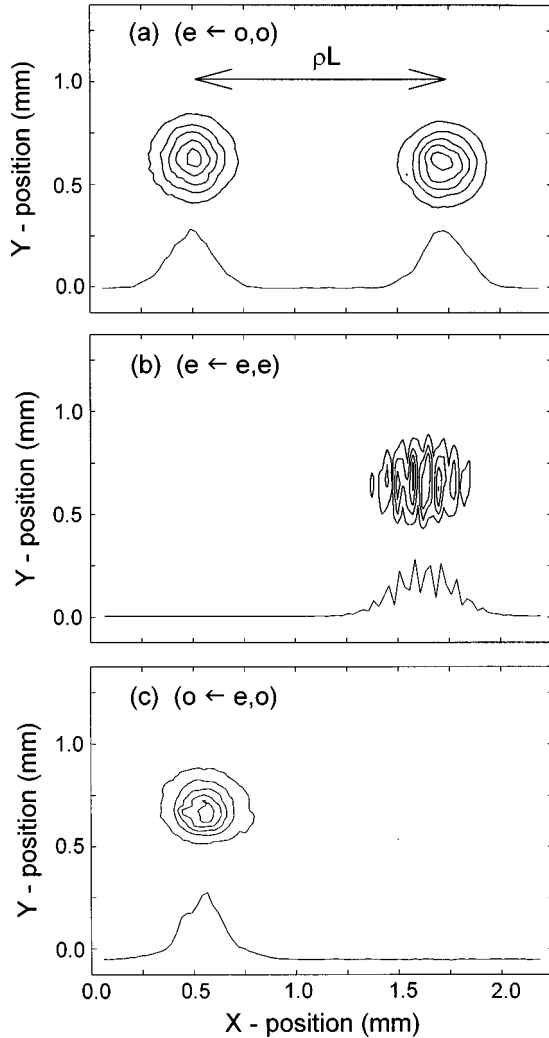


Fig. 3. Contour plots of second-harmonic fluence at the exit face of 19-mm-long LiIO_3 crystal ($\theta = 23^\circ$, $\alpha = 12.55^\circ$). The fundamental beam diameter is 0.2 mm, and the calculated e -wave birefringent walk-off is 1.2 mm. Plot (a) is for $(e \leftarrow o, o)$ with a coherence length of $38.5 \mu\text{m}$. The left beam is the driven wave created at the crystal exit face by the undisplaced o -polarized fundamental, and the right beam is the free wave created at the crystal input face and displaced by walk-off. Plot (b) is for $(e \leftarrow e, e)$ with a coherence length of $14.3 \mu\text{m}$. Both the free and driven waves are displaced by walk-off and overlap at the crystal exit face to create an interference pattern owing to the variation of crystal length across the beam plus the differing wavelengths within the crystal. Plot (c) is for $(o \leftarrow e, o)$ with a coherence length of $12.2 \mu\text{m}$. The undeviated o -polarized free wave generated at the crystal input face is evident, but the driven wave is absent because the e - and o -polarized fundamental beams do not overlap at the exit face.

relative to the absolute measurement of $(e \leftarrow o, o)$, assuming $d_{zzz} \approx d_{zxx}$ as reported by Jerphagnon¹⁷ and Choy and Byer.⁶ Our measured d_{eff} 's are listed in Table 8 along with values deduced from the literature. Note that our measurements do not provide a sensitive measure of d_{zzz} , as it contributes only $\sim 8\%$ to d_{eff} for $(e \leftarrow e, e)$.

In our previous discussion of the influence of walk-off, we claimed the free wave could be considered generated at the crystal input face, and the driven wave generated at the output face. For the $(e \leftarrow o, o)$ process we expect the second-harmonic at the exit face of the LiIO_3 crystal to consist of the free wave displaced by $\rho_{2\omega}L$ ($=1.16$ mm) from the fundamental beam, plus a nearly identical undisplaced driven wave. This is indeed the case, as illustrated in Fig. 3(a), which shows contour plots of the second-harmonic fluence at the exit face when the weakly focused 0.2-mm-diameter fundamental beam is o polarized. The exit face of the 19-mm-long crystal is imaged onto a CCD camera, passing only the second-harmonic light. For the $(e \leftarrow e, e)$ process, we expect the free wave to again be displaced by $\rho_{2\omega}L$ and the driven wave to also be displaced by $\rho_{\omega}L$. Because the two walk-off angles $\rho_{2\omega}$ and ρ_{ω} are nearly equal, the free and driven waves should overlap and interfere. This is demonstrated in Fig. 3(b). Note that there are about six interference fringes across the harmonic beam, causing clean angular separation of the free and driven waves as they propagate beyond the crystal. Finally, for the $(e \leftarrow o, e)$ process, the driven wave disappears because the two fundamental beams are completely separated by birefringent walk-off at the crystal exit face, causing the driving-harmonic polarization to disappear there as well. This is shown in Fig. 3(c), which shows the harmonic beam profile at the exit face for o -polarized harmonic light when the fundamental is linearly polarized at 45° to the e and o axes.

7. RELATIVE SIGNS OF d_{ij} 's

Determination of the relative signs of some of the d_{ij} 's is quite straightforward with our method. As an illustration we consider crystals of symmetry $3m$, a category that includes LiNbO_3 and $\beta\text{-BaB}_2\text{O}_4$ (see Table 2). Assuming Kleinman symmetry, the form of the nonlinear tensor is

$$d = \begin{bmatrix} 0 & 0 & 0 & 0 & d_{xxz} & -d_{yyy} \\ -d_{yyy} & d_{yyy} & 0 & d_{xxz} & 0 & 0 \\ d_{xxz} & d_{xxz} & d_{zzz} & 0 & 0 & 0 \end{bmatrix}. \quad (28)$$

There are three independent coefficients whose signs and magnitudes must be determined to characterize the crystal. The magnitudes and relative signs of the pair d_{xxz} ($=d_{yyy}$) and d_{zzz} can be found by use of a crystal cut for propagation along the x axis with the exit face tilted in either the xy or xz plane. With fundamental light polarized in the y and z directions respectively, and measurement of the z -polarized second harmonic, the magnitudes of d_{xxz} and d_{zzz} can be found by our method as described above. The relative signs of the two coefficients can be determined by noting the behavior of the free-wave en-

ergy as the linear input polarization is rotated by ψ measured from z polarization to y polarization. The free wave has contributions from both ($z \leftarrow y, y$) and ($z \leftarrow z, z$) processes, giving a net field

$$E_{\text{free}} = \left[\frac{d_{zyy} E_{\omega}^2 \sin^2 \psi}{n_{2\omega,z}^2 - n_{\omega,y}^2} \left(\frac{n_{\omega,y} + 1}{n_{2\omega,z} + 1} \right) \left| \frac{2}{n_{\omega,y} + 1} \right|^2 \right. \\ \left. + \frac{d_{zzz} E_{\omega}^2 \cos^2 \psi}{n_{2\omega,z}^2 - n_{\omega,z}^2} \left(\frac{n_{\omega,z} + 1}{n_{2\omega,z} + 1} \right) \left| \frac{2}{n_{\omega,z} + 1} \right|^2 \right] t_{2\omega}. \quad (29)$$

If the signs of the two terms inside the brackets are the same, the strength of the free wave does not pass through zero as the polarization is rotated, whereas it does if the signs are opposite. The generalization of this example is that choosing an eigen polarization of the free harmonic wave selects one row of the d tensor, while rotating the polarization of the fundamental can reveal the relative signs of some elements within that row.

Relative signs within a column can be determined with driven waves. For the same example of the class $3m$ crystals, if the fundamental is y polarized, the second column of the nonlinear tensor is selected. There are two nonzero elements in that column, d_{xxz} ($=d_{yyz}$) and d_{yyy} . If they have the same sign, the driven wave will be linearly polarized at an angle $90^\circ > \psi > 0^\circ$, where ψ is measured from the z axis toward the y axis. If the signs are opposite, the polarization angle will satisfy $-90^\circ < \psi < 0^\circ$.

We illustrate the measurement of relative signs within a row using our LiIO_3 sample. This is slightly more complex than the cases just described because propagation is along $0 = 23^\circ$ rather than along an optical axis. (Note that $\theta + \rho = 26.5^\circ$.) The e -polarized harmonic is selected so there are potential contributions from processes ($e \leftarrow o, o$) and ($e \leftarrow e, e$). In this case the two contributions to the free wave owing to ($d_{\text{eff}} = d_{xxz} \sin 26.5^\circ$) and ($d_{\text{eff}} = 3d_{xxz} \cos^2 26.5^\circ \sin 26.5^\circ + d_{zzz} \sin^3 26.5^\circ$) have the same sign if the fundamental light is linearly polarized, and the solid-curve plot of Fig. 4 shows the resulting lack of a destructive interference null. The harmonic signal is nearly independent of ψ because the values of $d_{\text{eff}}/\Delta k$ are nearly equal for the two processes. Had the signs been opposite, we would have seen a null. We simulated this by inserting a quarter-wave plate, aligned with its slow axis along the ($x-z$) direction, between the crystal and the half-wave plate that rotates the linear fundamental polarization. This retards the ($x-z$)-polarized fundamental by 90° relative to the y -polarized fundamental, reversing the sign of E^2 for the ($x-z$)-polarized fundamental but not for the y -polarized fundamental. The result is the dashed curve in Fig. 4 showing the expected null.

In LiIO_3 , columns four and five of the nonlinear tensor have multiple entries so a comparison of relative signs within columns can also be illustrated with LiIO_3 , but the rotations are expected to be small because d_{xyz} is twenty times smaller than d_{xxz} . Driven waves associated with processes ($o \leftarrow o, e$) and ($e \leftarrow o, e$) emerge at the same angle, and a measurement of the harmonic polarization angle of this beam yields relative signs of d_{eff} for these

two processes. They are proportional to d_{xyz} and d_{xxz} respectively, so a tilt of the driven-wave polarization toward the y axis would indicate the same sign for the two coefficients of column four. We measured a tilt of 4.5° in this direction indicating that the signs are the same. The magnitude of the tilt is in reasonable agreement with the expected 5.8° . Note that the relative signs of these two d_{eff} 's are dependent on crystal orientation and so are not a fundamental characteristic of the crystal. A similar measurement of the driven waves associated with ($o \leftarrow e, e$) and ($e \leftarrow e, e$) reveals a tilt of $\sim 0.5^\circ$ in the opposite direction, in accord with expectations.

8. OTHER CRYSTALS

Tables 1 and 2 list values of $|d_{\text{eff}}|$ for crystals of symmetry groups 6 (LiIO_3), $6mm$ (CdSe), $\bar{4}2m$ (KDP and isomorphs, AgGaS_2 , AgGaSe_2 , ZnGeP_2 , CdGeAs_2), and $3m$ ($\beta\text{-BaB}_2\text{O}_4$, LiNbO_3). Here X, Y , and Z refer to standard frames¹⁸ in which the optic axis of these uniaxial crystals is Z . Angle θ is the polar angle relative to the optical axis for uniaxial crystals, and ϕ is the azimuthal angle measured from the XZ plane toward the XY plane.¹

Crystals belonging to symmetry group $mm2$ (LBO , KNbO_3 , KTP , and isomorphs) have nonzero d_{XXZ} , d_{ZXX} , d_{YYZ} , d_{ZYY} , and d_{ZZZ} . The association between the standard reporting axis system (X, Y, Z) and the refractive index (optical) system, defined as the right-handed axis system in which $n_x < n_y < n_z$, is not unique in the literature,¹⁸ so, to avoid ambiguity, we write the d tensor in terms of the d coefficients in the optical frame. Tables 3–5 show d_{eff} for KTP and its isomorphs, for KNbO_3 , and for LBO , assuming propagation in one of the principal planes. The notations e and o represent extraordinary and ordinary polarizations for that particular principal plane, and angle θ is measured from the z axis, while ϕ is measured from the x axis. For example, in x -cut KTP , selection of fundamental and harmonic polarizations permits independent measurements of d_{zyy} via ($e \leftarrow o, o$), d_{zzz} via ($e \leftarrow o, o$), and d_{yyz} via ($o \leftarrow o, e$). Similarly, a

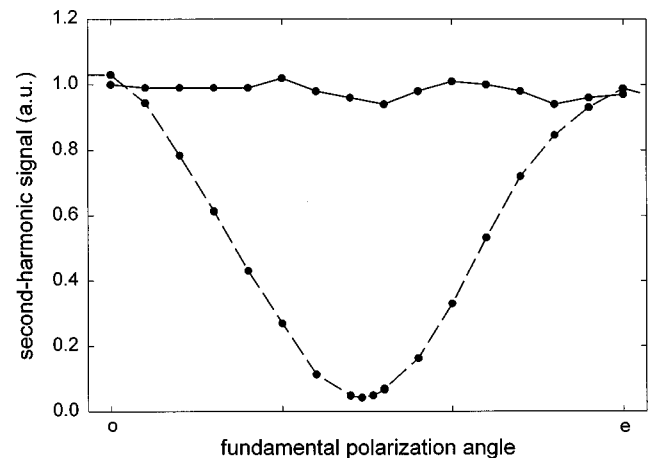


Fig. 4. Second-harmonic pulse energy in the e -polarized free beam versus the polarization angle of the fundamental light. The solid curve taken without the quarter-wave plate shows that d_{eff} has the same sign for ($e \leftarrow e, e$) and ($e \leftarrow o, o$). The dashed curve taken with the quarter-wave plate simulates oppositely signed d_{eff} 's.

y-cut sample yields d_{zzz} , d_{zxx} , and d_{xxz} . A single crystal can be cut to satisfy both of these orientations by beveling two sides. In the absence of dispersion of the nonlinear coefficients (Kleinman symmetry), permutation of the indexes of d_{ijk} leaves the value of d unchanged, so independent measurements of d_{yyz} and d_{zyy} or of d_{xxz} and d_{zxx} are not always necessary. However, processes mediated by these nominally equal coefficients have different values of Δk , permitting a trade-off between beam separation that increases with Δk and signal strength that decreases with Δk .

9. CONCLUSION

We demonstrated a general method of measuring Δk and d_{ijk} using nonphase-matched second-harmonic generation in thick, wedged nonlinear optical crystals. It is a clean method in the sense that d_{eff} can be related directly to measured input fundamental and output harmonic pulse energies without the complications of etalon effects in the sample, angular dependence of d_{eff} , or complicated entrance and exit-face boundary conditions. The strength of the second-harmonic signals is about the same as in the Maker-fringe method. We showed that our method is independent of birefringent or group-velocity walk-off, as long as the walk-off lengths are many coherence lengths. Further, no analysis of interference fringes is necessary, and multiple mixing processes can sometimes be measured simultaneously. Additionally, $n_{2\omega}$, \bar{n}_ω , and Δk can be measured with the same crystal via angular deflections of the beams emerging from the prism sample, although precise values for these can often be found in the literature. The method is also conducive to relating the signs of the nonlinear tensor elements with minimal analysis.

ACKNOWLEDGMENTS

This work was supported by the U.S. Department of Energy under contract DE-AC04-94AL85000. Sandia is a multiprogram laboratory operated by Sandia Corporation, a Lockheed Martin Company, for the U.S. Department of Energy.

REFERENCES

1. R. L. Sutherland, *Handbook of Nonlinear Optics* (Dekker, New York, 1996).
2. P. D. Maker, R. W. Terhune, M. Nisenoff, and C. M. Savage, "Effects of dispersion and focusing on the production of optical harmonics," *Phys. Rev. Lett.* **8**, 21–22 (1962).
3. J. Jerphagnon and S. K. Kurtz, "Maker fringes: a detailed comparison of theory and experiment for isotropic and uniaxial crystals," *J. Appl. Phys.* **41**, 1667–1681 (1970).
4. W. N. Herman and L. M. Hayden, "Maker fringes revisited: second-harmonic generation from birefringent or absorbing materials," *J. Opt. Soc. Am. B* **12**, 416–427 (1995).
5. D. Chemla and P. Kupecek, "Analyse des experiences de generation de second harmonique," *Rev. Phys. Appl.* **6**, 31–50 (1971).
6. M. M. Choy and R. L. Byer, "Accurate second-order susceptibility measurements of visible and infrared nonlinear crystals," *Phys. Rev. B* **14**, 1693–1706 (1976).
7. R. Morita, T. Kondo, Y. Kaneda, A. Sugihashi, N. Ogasawara, S. Umegaki, and R. Ito, "Multiple-reflection effects in optical second-harmonic generation," *Jpn. J. Appl. Phys.* **27**, L1134–L1136 (1988).
8. I. Shoji, T. Kondo, A. Kitamoto, M. Shirane, and R. Ito, "Absolute scale of second-order nonlinear-optical coefficients," *J. Opt. Soc. Am. B* **14**, 2268–2294 (1997).
9. Y. Yamamoto, T. Ashida, S. Kurimura, and Y. Uesu, "Two-dimensional observation of the Maker fringe and its application to the poling state evaluation of ferroelectric domains," *Appl. Opt.* **36**, 602–605 (1997).
10. S. Kurimura and Y. Uesu, "Application of the second-harmonic generation microscope to nondestructive observation of periodically poled ferroelectric domains in quasi-phase-matched wavelength converters," *J. Appl. Phys.* **81**, 369–375 (1997).
11. N. Bloembergen and P. S. Pershan, "Light waves at the boundary of nonlinear media," *Phys. Rev.* **128**, 606–622 (1962).
12. N. Okamoto, Y. Hirano, and O. Sugihara, "Precise estimation of nonlinear-optical coefficients for nonlinear films with $C_{\infty v}$ symmetry," *J. Opt. Soc. Am. B* **9**, 2083–2087 (1992).
13. A. V. Smith and M. S. Bowers, "Phase distortions in sum- and difference-frequency mixing in crystals," *J. Opt. Soc. Am. B* **12**, 49–57 (1995); A. V. Smith, W. J. Alford, T. D. Raymond, and M. S. Bowers, "Comparison of a numerical model with measured performance of a seeded, nanosecond KTP optical parametric oscillator," *J. Opt. Soc. Am. B* **12**, 2253–2276 (1995). SNLO freeware for modeling χ^2 nonlinear optics is available from A. V. Smith.
14. V. G. Dmitriev, G. G. Gurzadyan, and D. N. Nikogosyan, *Handbook of Nonlinear Optical Crystals* (Springer, New York, 1997).
15. K. Kato, "High-power difference-frequency generation at 4.4–5.7 μm in LiIO_3 ," *IEEE J. Quantum Electron.* **QE-21**, 119–120 (1985).
16. M. Okada and S. Ieiri, "Kleinman's symmetry relation in non-linear optical coefficient of LiIO_3 ," *Phys. Lett. A* **34**, 63–64 (1971).
17. J. Jerphagnon, "Optical nonlinear susceptibilities of lithium iodate," *Appl. Phys. Lett.* **16**, 298–299 (1970).
18. D. A. Roberts, "Simplified characterization of uniaxial and biaxial nonlinear optical crystals: a plea for standardization of nomenclature and conventions," *IEEE J. Quantum Electron.* **28**, 2057–2074 (1992).
19. R. C. Eckardt, H. Masuda, Y. X. Fan, and R. L. Byer, "Absolute and relative nonlinear optical coefficients of KDP, KD^*P , BaB_2O_4 , LiIO_3 , $\text{MgO}:\text{LiNbO}_3$, and KTP measured by phase-matched second-harmonic generation," *IEEE J. Quantum Electron.* **26**, 922–933 (1990).
20. G. Nath and S. Haussühl, "Large nonlinear optical coefficient and phase matched second harmonic generation in LiIO_3 ," *Appl. Phys. Lett.* **14**, 154–156 (1969).
21. A. J. Campillo and C. L. Tang, "Spontaneous parametric scattering of light in LiIO_3 ," *Appl. Phys. Lett.* **16**, 242–244 (1970).